

Multiple Antiferromagnetic Spin Fluctuations and Novel Evolution of T_c in Iron-Based Superconductors $\text{LaFe}(\text{As}_{1-x}\text{P}_x)(\text{O}_{1-y}\text{F}_y)$ Revealed by ^{31}P -NMR Studies

Takayoshi Shiota¹, Hidekazu Mukuda^{1*}, Masahiro Uekubo², Fuko Engetsu¹, Mitsuharu Yashima¹, Yoshio Kitaoka¹, Kwing To Lai², Hidetomo Usui², Kazuhiko Kuroki², Shigeki Miyasaka^{2†}, and Setsuko Tajima²

¹Graduate School of Engineering Science, Osaka University, Toyonaka, Osaka 560-8531, Japan

²Graduate School of Science, Osaka University, Toyonaka, Osaka 560-0043, Japan

(Received *****)

We report on ^{31}P -NMR studies of $\text{LaFe}(\text{As}_{1-x}\text{P}_x)(\text{O}_{1-y}\text{F}_y)$ over wide compositions for $0 \leq x \leq 1$ and $0 \leq y \leq 0.14$, which provide clear evidence that antiferromagnetic spin fluctuations (AFMSFs) are one of the indispensable elements for enhancing T_c . Systematic ^{31}P -NMR measurements revealed two types of AFMSFs in the temperature evolution, that is, one is the AFMSFs that develop rapidly down to T_c with low-energy characteristics, and the other, with relatively higher energy than the former, develops gradually upon cooling from high temperature. The low-energy AFMSFs in low y (electron doping) over a wide x (pnictogen height suppression) range are associated with the two orbitals of $d_{xz/yz}$, whereas the higher-energy ones for a wide y region around low x originate from the three orbitals of d_{xy} and $d_{xz/yz}$. We remark that the nonmonotonic variation of T_c as a function of x and y in $\text{LaFe}(\text{As}_{1-x}\text{P}_x)(\text{O}_{1-y}\text{F}_y)$ is attributed to these multiple AFMSFs originating from degenerated multiple $3d$ orbitals inherent to Fe-pnictide superconductors.

Since the discovery of superconductivity (SC) in a layered iron(Fe)-pnictide $\text{LaFeAs}(\text{O}_{1-y}\text{F}_y)$,¹ a number of researches have unraveled a rich variety of antiferromagnetic (AFM), structural, and SC phase diagrams in various Fe-pnictide families.² The SC transition temperature (T_c) of $\text{LaFe}(\text{As}_{1-x}\text{P}_x)(\text{O}_{1-y}\text{F}_y)$ exhibits a unique nonmonotonic variation, as shown in Fig. 1, where the respective compositions x and y control the local lattice parameter of the Fe-pnictogen (Pn) tetrahedron (x) through the isovalent substitution of As with P and an electron-doping level (y) through the substitution of O^{2-} with F^- .³⁻⁷ Previous NMR studies of this series ($0 \leq y \leq 0.1$) revealed that the AFM spin fluctuations (AFMSFs) are markedly enhanced at x where T_c exhibits a peak.⁸ The appearance of such unexpected AFMSFs was related to a reemergent AFM order phase at $(x, y) = (0.6, 0)$, denoted as AFM2 in Fig. 1, which is separated from the AFM1 at the parent LaFeAsO of $(x, y) = (0, 0)$.^{9,10} These results indicate that the AFMSFs are one of the important factors for enhancing the T_c in Fe-pnictide SCs, even when the lattice parameters deviate from their optimum values for a FePn_4 regular tetrahedron.^{11,12}

On the other hand, the AFMSFs are not so distinct at low energies for the compounds with a high T_c (~ 50 K), which are characterized by the local lattice parameters of FeAs_4 close to the regular tetrahedron.¹³⁻¹⁶ It has been reported that once further electrons are doped in the hydrogen-substituted $\text{LaFeAs}(\text{O}_{1-y'}\text{H}_{y'})$, the new phases of SC and AFM orders are uncovered and denoted as SC3 and AFM3 in Fig. 1, respectively.^{17,18} The theory has pointed out that the electronic state for the onset of SC3 resembles that of the highest T_c (≥ 50 K)

state.¹⁹ Thus, further systematic studies over wide compositions of x and y in $\text{LaFe}(\text{As}_{1-x}\text{P}_x)(\text{O}_{1-y}\text{F}_y)$ will provide an opportunity to unravel the universal relationship between the presence of AFMSFs and the onset of SC, including the unexpected relationship between the complicated effect of some electron doping and the deformation of the local structure of FePn_4 .

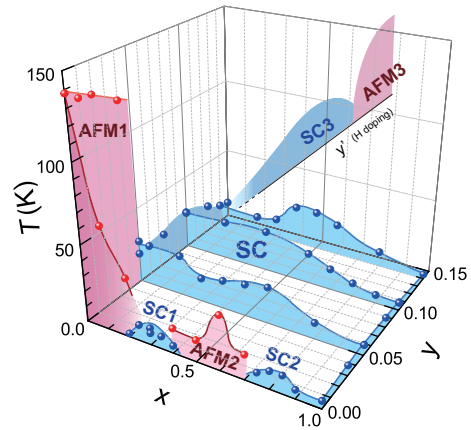


Fig. 1. (Color online) Superconducting and antiferromagnetic phase diagram of $\text{LaFe}(\text{As}_{1-x}\text{P}_x)(\text{O}_{1-y}\text{F}_y)$ for $y=0.14$ (Uekubo *et al.*⁷) and $0 \leq y \leq 0.10$,^{1-6,9,10} together with schematic phases of SC3 and AFM3 for $\text{LaFeAs}(\text{O}_{1-y'}\text{H}_{y'})$.^{17,18}

In this Letter, we report on ^{31}P -NMR studies of $\text{LaFe}(\text{As}_{1-x}\text{P}_x)(\text{O}_{1-y}\text{F}_y)$ over wide compositions for $0 \leq x \leq 1$ and $0 \leq y \leq 0.14$, revealing that AFMSFs are one of the indispensable elements for enhancing T_c . Systematic measurements of the ^{31}P nuclear spin relaxation rate ($1/T_1$) have revealed that the multiple AFMSFs relevant to the multiple-orbital nature of Fe-pnictides are respon-

*E-mail: mukuda@mp.es.osaka-u.ac.jp

†E-mail: mivasaka@phys.sci.osaka-u.ac.jp

sible for increasing T_c over wide compositions of x and y . As a result, we remark that a nonmonotonic variation of T_c in $\text{LaFe}(\text{As}_{1-x}\text{P}_x)(\text{O}_{1-y}\text{F}_y)$ is attributed to the multiple AFMSFs originating from degenerated multiple $3d$ orbitals inherent to Fe-pnictides.

Detailed ^{31}P -NMR ($I=1/2$) measurements were performed on coarse-powder polycrystalline samples of $\text{LaFe}(\text{As}_{1-x}\text{P}_x)(\text{O}_{0.86}\text{F}_{0.14})$ with nominal contents at $x=0.2, 0.4, 0.6$, and 1.0 . These samples were synthesized by the solid-state reaction method.^{5,7} Powder X-ray diffraction measurements indicated that the lattice parameters exhibit a monotonic variation with x .⁷ T_c s were determined from an onset of SC diamagnetism in the susceptibility measurement, as shown in Fig. 1.⁷ Extensive studies over a wide composition of $\text{LaFe}(\text{As}_{1-x}\text{P}_x)(\text{O}_{1-y}\text{F}_y)$ were also performed on the samples of $(x, y)=(0.2, 0.05)$ and $(x, y)=(0.2, 0.1)$. The Knight shift K was measured at a magnetic field of ~ 11.93 T, which was calibrated using a resonance field of ^{31}P in H_3PO_4 . Generally, K comprises the temperature(T)-dependent spin shift $K_s(T)$ and the T -independent chemical shift K_{chem} , expressed as $K = K_s(T) + K_{\text{chem}}$. The nuclear-spin lattice-relaxation rate $^{31}(1/T_1)$ of ^{31}P -NMR was measured at the field of ~ 11.93 T by fitting a recovery curve for ^{31}P nuclear magnetization to a single exponential function $m(t) \equiv [M_0 - M(t)]/M_0 = \exp(-t/T_1)$. Here, M_0 and $M(t)$ are the respective nuclear magnetizations for a thermal equilibrium condition and at time t after a saturation pulse.

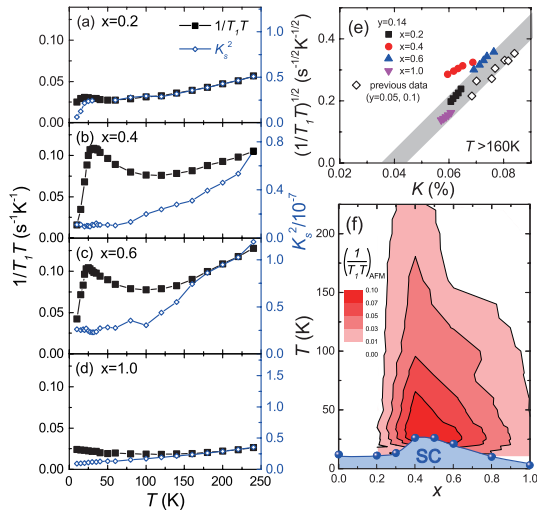


Fig. 2. (Color online) T dependences of $(1/T_1T)$ and $K_s^2(T)$ for (a) $x=0.2$, (b) $x=0.4$, (c) $x=0.6$, and (d) $x=1.0$ of $\text{LaFe}(\text{As}_{1-x}\text{P}_x)(\text{O}_{0.86}\text{F}_{0.14})$. (e) Plot of $(1/T_1T)^{1/2}$ vs K with an implicit parameter of T for these compounds, using data at high temperatures ($T \geq 160$ K). The empty diamonds are the previous data on $y=0.05$ and 0.1 ($T=200$ K).^{8,10} The data for $x=0.4$ deviate from this line owing to the development of AFMSFs. (f) Contour plot of $(1/T_1T)_{\text{AFM}}$ for $y=0.14$, indicating that the AFMSFs significantly develop where T_c exhibits a peak.

Figures 2(a)-2(d) show the T dependences of $(1/T_1T)$ and $K_s^2(T)$ ($= (K - K_{\text{chem}})^2$) for $x=0.2, 0.4, 0.6$, and 1.0 . The plot of $(1/T_1T)^{1/2}$ against $K(T)$, as shown in Fig. 2(e), enables us to obtain K_s by evaluat-

ing K_{chem} to be $0.04(\pm 0.01)\%$ for these compounds. Here, note that the data at temperatures higher than $T \sim 160$ K are used since the contribution of AFMSFs in $(1/T_1T)$ is negligible. The value of K_{chem} is comparable to those evaluated in previous studies.^{8,10,16} $K_s(T)$ is proportional to $\chi(q=0)$ with the relation $K_s(T) = A_{\text{hf}}(0)\chi(q=0) \propto A_{\text{hf}}(0)N(E_F)$. Here, $\chi(q=0)$ is the static spin susceptibility, $A_{\text{hf}}(0)$ is the hyperfine coupling constant at $q=0$, and $N(E_F)$ is the density of states (DOS) at the Fermi level (E_F).

As for $x=0.2$ and 1.0 , the T dependence of $(1/T_1T)$ follows that of $K_s^2(T)$ for a wide T region, as shown in Figs. 2(a) and 2(d), which point to the Korringa's relation $(1/T_1T) \propto N(E_F)^2$ expected for conventional metals. By contrast, the $(1/T_1T)$ s at $x=0.4$ and 0.6 increase as temperature decreases, although $K_s(T)$ s decrease as shown in Figs. 2(b) and 2(c). This contrasted behavior between $(1/T_1T)$ and $K_s(T)$ demonstrates the development of AFMSFs with finite wave vectors as temperature decreases. To deduce the development of AFMSFs following the previous studies,^{8,10,16} we assume that $(1/T_1T)$ is decomposed as

$$(1/T_1T) = (1/T_1T)_{\text{AFM}} + (1/T_1T)_0,$$

where the first term represents the contribution of AFMSFs with the finite wave vectors Q presumably around $(0, \pi)$ and $(\pi, 0)$ that significantly develop upon cooling, and the second one represents the q -independent one in proportion to $N(E_F)^2$. Figure 2(f) shows a contour plot of $(1/T_1T)_{\text{AFM}}$ for $y=0.14$, which is illustrated by assuming that the T dependence of $(1/T_1T)_0$ is identical to that of $K_s^2(T)$. This contour shows that the AFMSFs develop upon cooling for $x=0.4$ and 0.6 exhibiting relatively high T_c values; by contrast, they are markedly suppressed for $x=0.2$ and 1.0 exhibiting very low T_c values.

Figure 3(a) shows the contour plots of $(1/T_1T)_{\text{AFM}}$ for $0 \leq y \leq 0.14$ in a common scale. The AFMSFs play a significant role in raising T_c for wide compositions of x and y . Here, note that there are two types of AFMSFs in the T -evolution upon cooling. Namely, focusing on the T -variation of $(1/T_1T)_{\text{AFM}}$ for the two samples of $y=0.05$, Fig. 3(b) indicates that the AFMSFs at $x=0.6$ largely develop only at low temperatures, whereas those at $x=0.2$ gradually develop upon cooling from high temperatures. To gain further insight into these features of the AFMSFs, we define T_{SF} as the temperature below which AFMSFs start to develop, and $(1/T_1T)_{\text{AFM}}^{\text{max}}$ as the maximum value of $(1/T_1T)_{\text{AFM}}$, as presented in Fig. 3(b). $(1/T_1T)_{\text{AFM}}$ dominated by AFMSFs with a wave vector Q is generally described as

$$\left(\frac{1}{T_1T}\right)_{\text{AFM}} \propto \lim_{\omega \rightarrow \omega_0 \sim 0} |A_{\text{hf}}(Q)|^2 \frac{\chi''(Q, \omega)}{\omega},$$

where $A_{\text{hf}}(Q)$ is the hyperfine-coupling constant at $q = Q$, $\chi(Q, \omega)$ is the dynamical spin susceptibility at $q = Q$ and energy ω , and ω_0 is an NMR frequency approximating as $\omega_0 \sim 0$. Thus, the $(1/T_1T)_{\text{AFM}}^{\text{max}}$ probes a low energy limit of $\chi''(Q, \omega)/\omega$ around $\omega_0 \sim 0$, representing how large the spectral weight of AFMSFs are at low energies. The T_{SF} indicates the temperature that

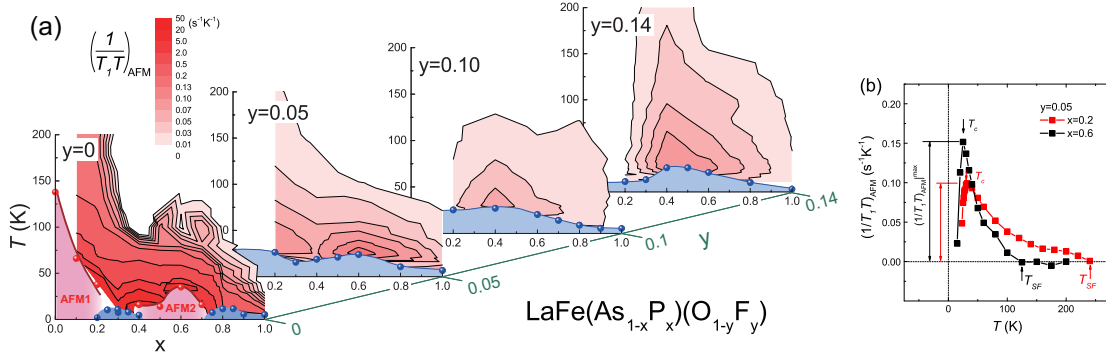


Fig. 3. (Color online) (a) Contour plots of $(1/T_1T)_{\text{AFM}}$ for $y=0.0$,¹⁰ 0.05, 0.10,⁸ and 0.14 in a common scale, providing clear evidence that the AFMSFs play a significant role in raising T_c for the present compositions of x and y . (b) Typical T dependence of $(1/T_1T)_{\text{AFM}}$ at $x=0.2$ and 0.6 for $y=0.05$. The AFMSFs at $x=0.2$ gradually develop upon cooling from higher temperature, whereas the AFMSFs at $x=0.6$ develop rapidly only at low temperature, although the value of $(1/T_1T)_{\text{AFM}}$ at low temperature is smaller in the former case than in the latter case. We define T_{SF} as the temperature below which the AFMSFs start to develop, and $(1/T_1T)_{\text{AFM}}^{\text{max}}$ as the maximum value of $(1/T_1T)_{\text{AFM}}$.

$\chi''(Q, \omega)$ significantly starts to increase upon cooling, roughly pointing to a characteristic energy of AFMSFs.

Note that the curves A, B, and C in Fig. 4(a) are along the values of T_c being relatively high for the wide compositions of x and y .¹⁻⁷ Figures 4(b) and 4(c) show the contour plots of T_{SF} and $(1/T_1T)_{\text{AFM}}^{\text{max}}$, respectively. The curve A is along the high values of T_{SF} in Fig. 4(b), demonstrating that the development of AFMSFs below T_{SF} is mostly responsible for increasing T_c . Here, note that the high values of T_c are along the high values of T_{SF} , in other words, roughly along the high values of the characteristic energy of AFMSFs. In fact, the theory predicted that the three orbitals of $d_{xz}/yz + d_{xy}$ are relevant to the AFMSFs characteristic at finite energies rather than at low energies in association with the AFM1 order at $(x, y)=(0, 0)$.²⁰⁻²² On the other hand, the high values of T_c along the curve B are along the large values of $(1/T_1T)_{\text{AFM}}^{\text{max}}$, as shown in Fig. 4(c), demonstrating that the development of the AFMSFs at low energies is also responsible for increasing T_c , originating from the collapse of the AFM2 order at $(x, y)=(0.6, 0)$.^{9,10} Here, note that the very good nesting of the hole Fermi surfaces (FSs) at $\Gamma(0,0)$ and electron FSs at $M(0,\pi)(\pi,0)$ in the unfolded FS regime is dominated mostly by the two orbitals of d_{xz}/yz , bringing about the onset of the AFM2 order at $(x, y)=(0.6, 0)$.^{20,22} Hence, the present result suggests that these AFMSFs dominated by the two orbitals of d_{xz}/yz are gradually suppressed against the increase in the electron doping level as y increases from 0 to 0.14.

Theoretically, two different types of the T -evolution of AFMSFs shown in Fig. 3(b) were consistently reproduced by the fluctuation-exchange (FLEX) approximation in the multi-orbital Hubbard model. In this model, Arai *et al.* revealed that the d_{xz}/yz -derived AFMSFs around the AFM2 phase are largely enhanced at low energies, whereas the $d_{xz}/yz + d_{xy}$ derived AFMSFs around the AFM1 are characteristic at finite energies rather than at low energies.²⁰ In this context, it is notable that the highest $T_c=27$ K is denoted at $(x, y)=(0.4, 0.1)$ by a star in Fig. 4(a) around which the curves A and B merge. It is instructive to note that the increase in the character-

istic energy of AFMSFs from low to high energies brings about the increase in T_c . This event is consistent with the spin-fluctuations mediated SC mechanism, which enables us to calculate a possible value of T_c on the basis of the integration of the AFMSF spectrum over a wide energy range.

We also note that as seen in Fig. 4(a), the high value of T_c at $(x, y)=(0.4, 0.1)$ is kept along the curve C toward $(x, y)=(0.4, 0.14)$ at which the AFMSFs from low to high energies slightly recover, as deduced from Figs. 4(b) and 4(c). This event may be associated with a reemergence of the d_{xz}/yz -derived AFMSFs since the low pnictogen height at large x (~ 0.5) will cause the FSs of the d_{xy} orbital to sink below E_F and the nesting of FSs of d_{xz}/yz orbitals to become somewhat better.²² It is worth comparing this with the further electron-overdoped SC3 state in LaFeAs ($\text{O}_{1-y'}\text{H}_{y'}$)¹⁷ shown in Fig. 1, since no nesting of FSs is expected. In these compounds, note that the hole FS in association with the d_{xz}/yz orbitals significantly shrinks owing to the heavy electron doping, whereas there still remain the hole FS relevant to the d_{xy} orbital and the large electron FSs.¹⁷ According to the spin-fluctuation model,¹⁹ the prioritized diagonal hopping on the d_{xy} orbitals reenforces the other type of AFMSFs in the high- T_c state of the SC3 phase, which is dominated by the high-energy AFMSFs,²³ rather than the low-energy ones.²⁴ It is interesting to unravel the systematic relationship between T_c and the evolution of different types of AFMSFs in the series going from LaFe($\text{As}_{1-x}\text{P}_x$)(O_{1-y}F_y) to LaFeAs($\text{O}_{1-y'}\text{H}_{y'}$).

Finally, we remark on the variation of $N(E_F)$ over wide x and y regions, which can be seen from the contour plot of $K_s(T \rightarrow 0)$ estimated from an extrapolation to $T \rightarrow 0$, as shown in Fig. 4(d). Note that $K_s(T \rightarrow 0)$ is directly proportional to $\chi(q=0)$ or $N(E_F)$. As seen in the figure, $K_s(T \rightarrow 0)$ increases around $(x, y)=(1, 0)$ owing to the peak of DOS mainly arising from the $d_{3z^2-r^2}$ -derived three-dimensional hole pocket around $Z(\pi, \pi, \pi)$.^{10,25} In fact, this contour plot of $N(E_F)$ has no correlation with the T_c values. This indicates that the BCS-type SC mechanism through the electron-phonon interaction is not applicable even for the phosphorus-end members ($x=1.0$),

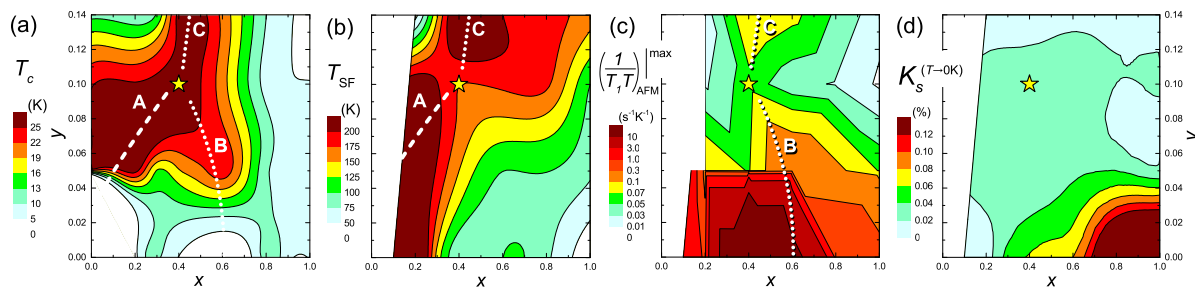


Fig. 4. (Color online) Contour plots of (a) T_c , $^{1-7}$ (b) T_{SF} , (c) $(1/T_1T)_{AFM}^{|\max|}$, and (d) $K_s(T \rightarrow 0)$ for wide compositions of x and y in $\text{LaFe}(\text{As}_{1-x}\text{P}_x)(\text{O}_{1-y}\text{F}_y)$. The definitions of T_{SF} and $(1/T_1T)_{AFM}^{|\max|}$ are shown in Fig. 3(b). The respective curves A and B correspond to the branch that T_{SF} is relatively high and the one that $(1/T_1T)_{AFM}^{|\max|}$ is relatively large. The star at $(x, y) = (0.4, 0.1)$ indicates the highest $T_c (= 27 \text{ K})$ point in the present compounds.

where the AFMSFs are significantly reduced and their T_c values are less than 10K.

In summary, the systematic ^{31}P -NMR measurements for $\text{LaFe}(\text{As}_{1-x}\text{P}_x)(\text{O}_{1-y}\text{F}_y)$ with $0 \leq x \leq 1$ and $0 \leq y \leq 0.14$ have unraveled two types of AFMSFs in the T -evolution upon cooling, that is, one is the AFMSFs that develops rapidly down to T_c with low-energy characteristics, and the other, with relatively higher energy than the former, develops gradually upon cooling from high temperature. The low-energy AFMSFs in low y (electron doping) over a wide x (pnictogen-height suppression) range are associated with the nesting effect of FSs dominated mostly by the two orbitals of $d_{xz/yz}$, whereas the higher-energy ones for a wide y region around low x originate from the three orbitals of d_{xy} and $d_{xz/yz}$.^{20,22} The intimate correlation between multiple AFMSFs and T_c values indicates that the AFMSFs are one of the indispensable elements for enhancing T_c , even though the lattice parameters deviate from their optimum values for the FePn_4 regular tetrahedron. We remark that the non-monotonic variation of T_c as a function of x and y in $\text{LaFe}(\text{As}_{1-x}\text{P}_x)(\text{O}_{1-y}\text{F}_y)$ is attributed to these multiple AFMSFs originating from degenerated multiple $3d$ orbitals inherent to Fe-pnictide superconductors.

This work was supported by Grants-in-Aid for Scientific Research (Nos. 26400356 and 26610102) from the Ministry of Education, Culture, Sports, Science and Technology (MEXT), Japan.

- 1) Y. Kamihara, T. Watanabe, M. Hirano, and H. Hosono, *J. Am. Chem. Soc.* **130**, 3296 (2008).
- 2) H. Hosono and K. Kuroki, *Physica C* **514**, 399 (2015).
- 3) H. Luetkens, H.-H. Klauss, M. Kraken, F. J. Litterst, T. Dellmann, R. Klingeler, C. Hess, R. Khasanov, A. Amato, C. Baines, M. Kosmala, O. J. Schumann, M. Braden, J. Hamann-Borrero, N. Leps, A. Kondrat, G. Behr, J. Werner, and B. Büchner, *Nat. Mater.* **8**, 305 (2009).
- 4) S. Saijo, S. Suzuki, S. Miyasaka, and S. Tajima, *Physica C* **470**, S298 (2010).
- 5) K. T. Lai, A. Takemori, S. Miyasaka, F. Engetsu, H. Mukuda, and S. Tajima, *Phys. Rev. B* **90**, 064504 (2014).
- 6) C. Wang, S. Jiang, Q. Tao, Z. Ren, Y. Li, L. Li, C. Feng, J. Dai, G. Cao, and Z. Xu, *Europhys. Lett.* **86**, 47002 (2009).
- 7) M. Uekubo, K. T. Lai, A. Takemori, S. Miyasaka, S. Tajima, R. Kumai, H. Nakao, and Y. Murakami, Submitted.
- 8) H. Mukuda, F. Engetsu, K. Yamamoto, K. T. Lai, M. Yashima, Y. Kitaoka, A. Takemori, S. Miyasaka, and S. Tajima, *Phys. Rev. B* **89**, 064511 (2014).
- 9) S. Kitagawa, T. Iye, Y. Nakai, K. Ishida, C. Wang, G. -H. Cao, and Z. -A. Xu, *J. Phys. Soc. Jpn.* **83**, 023707 (2014).
- 10) H. Mukuda, F. Engetsu, T. Shiota, K. T. Lai, M. Yashima, Y. Kitaoka, S. Miyasaka, and S. Tajima, *J. Phys. Soc. Jpn.* **83**, 083702 (2014).
- 11) C. H. Lee, A. Iyo, H. Eisaki, H. Kito, M. T. Fernandez-Diaz, T. Ito, K. Kihou, H. Matsushita, M. Braden, and K. Yamada, *J. Phys. Soc. Jpn.* **77**, 083704 (2008).
- 12) Y. Mizuguchi, Y. Hara, K. Deguchi, S. Tsuda, T. Yamaguchi, K. Takeda, H. Kotegawa, H. Tou, and Y. Takano, *Supercond. Sci. Technol.* **23**, 054013 (2010).
- 13) H. Mukuda, S. Furukawa, H. Kinouchi, M. Yashima, Y. Kitaoka, P. M. Shirage, H. Eisaki, and A. Iyo, *Phys. Rev. Lett.* **109**, 157001 (2012).
- 14) Y. Tomita, H. Kotegawa, Y. Tao, H. Tou, H. Ogino, S. Horii, K. Kishio, and J. Shimoyama, *Phys. Rev. B* **86**, 134527 (2012).
- 15) K. Yamamoto, H. Mukuda, H. Kinouchi, M. Yashima, Y. Kitaoka, M. Yogi, S. Sato, H. Ogino, and J. Shimoyama, *J. Phys. Soc. Jpn.* **81**, 053702 (2012).
- 16) M. Miyamoto, H. Mukuda, T. Kobayashi, M. Yashima, Y. Kitaoka, S. Miyasaka, and S. Tajima, *Phys. Rev. B* **92**, 125154 (2015).
- 17) S. Iimura, S. Matsuishi, H. Sato, T. Hanna, Y. Muraba, S. W. Kim, J. E. Kim, M. Takata, and H. Hosono, *Nat. Commun.* **3**, 943 (2012).
- 18) M. Hiraiishi, S. Iimura, K. M. Kojima, J. Yamaura, H. Hiraka, K. Ikeda, P. Miao, Y. Ishikawa, S. Torii, M. Miyazaki, I. Yamauchi, A. Koda, K. Ishii, M. Yoshida, J. Mizuki, R. Kadono, R. Kumai, T. Kamiyama, T. Otomo, Y. Murakami, S. Matsuishi, and H. Hosono, *Nat. Phys.* **10**, 300 (2014).
- 19) K. Suzuki, H. Usui, S. Iimura, Y. Sato, S. Matsuishi, H. Hosono, and K. Kuroki, *Phys. Rev. Lett.* **113**, 027002 (2014).
- 20) H. Arai, H. Usui, K. Suzuki, Y. Fuseya, and K. Kuroki, *Phys. Rev. B* **91**, 134511 (2015).
- 21) K. Kuroki, H. Usui, S. Onari, R. Arita, and H. Aoki, *Phys. Rev. B* **79**, 224511 (2009).
- 22) H. Usui, K. Suzuki, and K. Kuroki, *Sci. Rep.* **5**, 11399 (2015).
- 23) S. Iimura, S. Matsuishi, M. Miyakawa, T. Taniguchi, K. Suzuki, H. Usui, K. Kuroki, R. Kajimoto, M. Nakamura, Y. Inamura, K. Ikeuchi, S. Ji, and H. Hosono, *Phys. Rev. B* **88**, 060501(R) (2013).
- 24) R. Sakurai, N. Fujiwara, N. Kawaguchi, Y. Yamakawa, H. Kontani, S. Iimura, S. Matsuishi, and H. Hosono, *Phys. Rev. B* **91**, 064509 (2015).
- 25) T. Miyake, T. Kosugi, S. Ishibashi, and K. Terakura, *J. Phys. Soc. Jpn.* **79**, 123713 (2010).